Available online at www.sciencedirect.com

SciVerse ScienceDirect

Physics Procedia 37 (2012) 1389 – 1397

Physics Procedia

TIPP 2011 - Technology and Instrumentation in Particle Physics 2011

Seismic attenuation technology for the Advanced Virgo gravitational wave detector

M.G. Beker[1a], M. Blom[a], J.F.J. van den Brand[a,b], H.J. Bulten[a,b], E. Hennes[a], D.S. Rabeling[a,b]

[a]*Nikhef, National Institute for Subatomic Physics, Science Park 105, 1098 XG Amsterdam, The Netherlands*
[b]*VU University Amsterdam, Boelenlaan 1081, NL-1081 HV Amsterdam, The Netherlands*

Abstract

The current interferometric gravitational wave detectors are being upgraded to what are termed 'second generation' devices. Sensitivities will be increased by an order of magnitude and these new instruments are expected to uncover the field of gravitational astronomy. A main challenge in this endeavor is the mitigation of noise induced by seismic motion. Detailed studies with Virgo show that seismic noise can be reinjected into the dark fringe signal. For example, laser beam jitter and backscattered light limit the sensitivity of the interferometer.

Here, we focus on seismic attenuators based on compact inverted pendulums in combination with geometric anti-springs to obtain 40 dB of attenuation above 4 Hz in six degrees of freedom. Low frequency resonances (< 0.5 Hz) are damped by using a control system based on input from LVDTs and geophones. Such systems are under development for the seismic attenuation of optical benches operated both in air and vacuum. The design and realization of the seismic attenuation system for the Virgo external injection bench, including its control scheme, will be discussed and stand-alone performance presented.

Keywords: Virgo, seismic attenuation, geometric anti-spring, inverted pendulum

1. Introduction

Suppression of instrumental noise sources has been a major challenge in the development of interferometric gravitational wave (GW) detectors in the previous decades. As the detectors advance to increasingly more sensitive designs, different noise sources become dominant and need to be addressed. Within the next few years the current large-scale detectors will be upgraded, with the aim to improve sensitivity by a factor of 10 [1–3], bringing with it a range of instrumental noise challenges.

Seismic motion is a noise source that limits the sensitivity of GW detectors at low frequencies (below 100 Hz) [4]. Unwanted vibrations of optical components in the interferometer produce arm-length differences that directly induce noise at the interferometer output. To reach the desired sensitivity of the Virgo detector, suppression of seismic motion in the interferometer arm cavities and beam splitter, by up to 14 orders of

[1]Email: M.Beker@Nikhef.nl

 doi:10.1016/j.phpro.2012.03.741

magnitude, is required. This is achieved with 8 m high suspension systems called super attenuators [5]. The seismic requirements of other optical components are less stringent as these produce 'common mode' noise, the effects of which cancel at the beam splitter. However, due to effects of the laser beam jitter and backscattered light, noise from these components still finds its way into the interferometer output. One such category of optical components are the external benches. They are situated outside the vacuum system (hence the name 'external'), housing the optics to monitor the status and performance of the interferometer. The external injection bench (EIB) additionally supports the optics for the laser beam injection. Here we describe a compact system developed to isolate the EIB from seismic noise. It is known as the external injection bench seismic attenuation system (EIB-SAS).

Besides it's application in gravitational astronomy, EIB-SAS technology could also be implemented in a range of other fields including high energy physics. For example, luminosity requirements of next generation accelerators necessitate sub-nanometer interaction points, placing stringent requirements on accelerator vibration levels [6, 7].

1.1. The Virgo external injection bench

The Virgo EIB supports the optics responsible for the monitoring and final preparation of the laser light before it enters the vacuum system, and the monitoring of light reflected by the in-vacuum optics including the interferometer itself. The monitored signals are essential for the alignment and locking of the various cavities such as the input mode cleaner and reference cavity [1].

Seismic induced motion of the current bench couples seismic noise into the interferometer. Residual motion of the optics before injection into the vacuum results in laser beam jitter (movement of the input beam with respect to the interferometer axis) [8] and scattering of diffused light. The non-linear behavior of this coupling can also result in the up-conversion of low frequency seismic excitations (< 10 Hz) into the detection band (> 10 Hz) [9, 10].

Tests show that noise at the output of the interferometer can be attributed to the seismic motion of the EIB [11]. The measurements involved testing the coherence between seismic motion of the current bench and the output of the interferometer. Results of these tests are shown in Fig. 1. Seismic motion of the EIB induces noise in the interferometer output around 40 Hz, the resonance frequency of the current EIB supports. Large peaks are also visible from 100 - 1000 Hz. These can be attributed to resonances of the optics suspensions. The design sensitivity of Advanced Virgo, a second generation GW detector, is also shown in Fig. 1. It could be compromised by current EIB motion over a broad frequency range from 10 - 1000 Hz. EIB-SAS aims to mitigate amplification of seismic motion above 5 Hz.

2. Passive isolation with harmonic oscillators

There are two main strategies that can be pursued when it comes to seismic noise isolation; active and passive. Active damping involves broadband monitoring of seismic motion, the signals of which are analyzed for use in a feedback control system, to produce a corrective force on the to-be-isolated object. Active systems have been incorporated in the Advanced LIGO baseline design [2] for the (pre)isolation of its interferometer optics. Passive damping makes use of the mechanical second-order low-pass filter characteristics inherent to harmonic oscillators such as pendula and mass-spring systems. In general, passive isolators still require an active component to damp the system resonances, as described in section 3. The transfer function of a typical oscillator is given by,

$$\frac{x_1(\omega)}{x_0(\omega)} = \frac{\omega_0^2 + \beta\omega^2 + i\alpha(\omega)}{\omega_0^2 - \omega^2 + i\alpha(\omega)}, \tag{1}$$

where x_0 is the ground motion, x_1 the motion of the supported mass and β, a property of the mass distribution of the system. The term α accounts for the internal damping of the system where a constant α relates to structural damping, whilst viscous damping appears in a linearly frequency dependent $\alpha(\omega)$. Generally α and β are small and the transfer function drops off with $1/\omega^2$ above the resonance frequency, ω_0. As $\omega \to \infty$ the transfer function will plateau out to a value given by β.

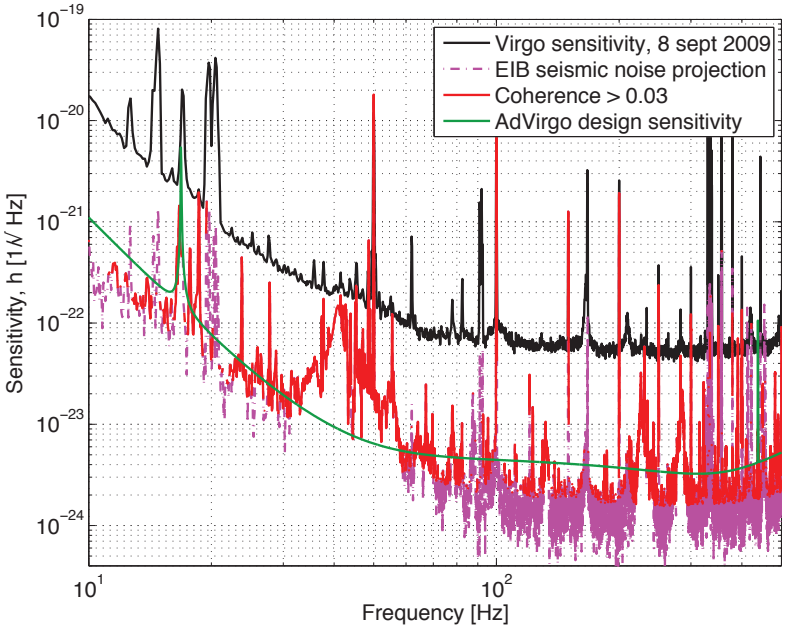

Fig. 1. Coherence measurements between detector output and seismic noise of the current external injection bench, adopted from [11]. The detector sensitivity (black curve) is plotted together with the seismic noise (dashed magenta curve). The seismic noise with a coherence above 0.03 is highlighted by the solid red curve. Seismic motion of the EIB induces the most noise into the interferometer output around 40 Hz. The design sensitivity of Advanced Virgo is also given by the solid green curve.

The lower the resonance frequency, the higher the attenuation factor at the frequencies of interest, above ω_0. Attenuation requirements therefore place constraints on ω_0. In basic mechanical oscillators such low resonance frequencies can only be reached with excessive and impractical parameters. For example, a 40 dB suppression at a few Hertz, requires a $f_0 < 100$ mHz. In the case of a simple pendulum, this would mean a length of 25 m ($\omega_0 = 2\pi f_0 = \sqrt{g/l}$).

This section will describe two types of harmonic oscillators that are implemented in EIB-SAS. Their design incorporates an anti-spring effect, allowing for low resonance frequencies in all degrees of freedom, while still having compact dimensions. An anti-spring is a system with a negative spring constant. That means that once disturbed out of equilibrium the system will keep on moving away from it's equilibrium point. The first to be discussed is the geometric anti-spring (GAS) followed by the inverted pendulum (IP). Finally the two concepts will be combined and EIB-SAS will be discussed in more detail.

2.1. The geometric anti-spring

A GAS filter, as shown in Fig. 2a, is a set of 8 radially positioned leaf springs, each supporting a load, F_y. They are radially compressed in such a way that the horizontal force they exert on each other results in a tunable anti-spring effect. In this way the vertical stiffness can be tuned to an arbitrarily low value. Fig. 2b shows a schematic of a single GAS blade.

The static properties of a GAS filter can be analytically derived, as was done by Cella et. al. [12]. It involves solving the following differential equation,

$$\frac{1}{L^2}\frac{d}{ds}\left[EI(s)\frac{d\theta}{ds}\right] = F_x \sin\theta(s) - F_y \cos\theta(s), \tag{2}$$

with boundary conditions, $\theta(0) = \theta_0$, $\theta(L) = \theta_L$, where $EI(s)$ is the flexural rigidity of the blade at distance s from the clamp, $\theta(s)$, the angle between horizontal and the tangent of the blade and L the length of the blade. F_x and F_y are the compression and load forces, respectively.

Finite element models of the GAS blades accurately reproduce the solutions to Eq. (2). The tunable spring constant properties of the GAS are evident in plots of these results for various compressional distances x_L. In Fig. 3a the blade tip height y_L is plotted as a function of the load supported by the GAS filter. The slope of these curves around the equilibrium point is the spring's vertical stiffness. The solid red curve corresponds to a well tuned stable GAS filter. If the blades are compressed even further, the system passes a critical point and becomes bistable. In this state the filter has multiple working positions for a given load and compression and will have an undefined resonance frequency. This can be seen in Fig. 3b where the corresponding resonance frequency for each point is plotted as a function of the blade tip vertical position. For increasing compression it is possible to tune the GAS filters to increasingly lower frequencies, up until the critical point, after which the frequencies become undefined.

2.2. The inverted pendulum

A simple IP, shown on the left of Fig. 4, made of a rigid rod, of mass m, supporting a mass M, is in itself an anti-spring [13]. By fixing it to the ground with a flexible pivot with a positive angular spring constant, k_θ, a quasi-stable system is obtained. By adjusting the supported mass it is possible to tune the resonance frequency,

$$\omega_0^2 = \frac{\frac{k_\theta}{l^2} - (M + \frac{m}{2})\frac{g}{l}}{M + \frac{m}{3}}. \tag{3}$$

For this simple IP, the level of the high frequency plateau resulting from Eq. (1) is given by, $\beta \approx \frac{m}{6M}$. This level can be tuned by adding counterweights on an extension of the IP rod that reaches below the flexible joint. This can be seen on the right hand side of Fig. 4.

2.3. The EIB seismic attenuation system

The EIB-SAS, shown in Fig. 5, consists of three GAS filters mounted into a rigid frame called the spring box. The spring box is supported by three IPs and free to move in all horizontal degrees of freedom. The optical bench is fixed to a plate that is in turn connected to the center points of the three GAS filters, allowing it to move in the remaining three vertical degrees of freedom. A plateau is connected rigidly to the ground and provides support for displacement sensors and actuators (see section 3.1). Stepping motors are used for DC positioning of the bench to within $\pm 20\ \mu$m.

3. Resonance frequency damping

We have seen that a harmonic oscillator can function as a mechanical second-order low pass filter. At the resonance frequencies, however, seismic motion can be amplified by up to several orders of magnitude, depending on the quality factor of the respective oscillator. For EIB-SAS an amplification of 30 dB is typical. The requirements for EIB-SAS demand a suppression of these modes by at least a factor of 10.

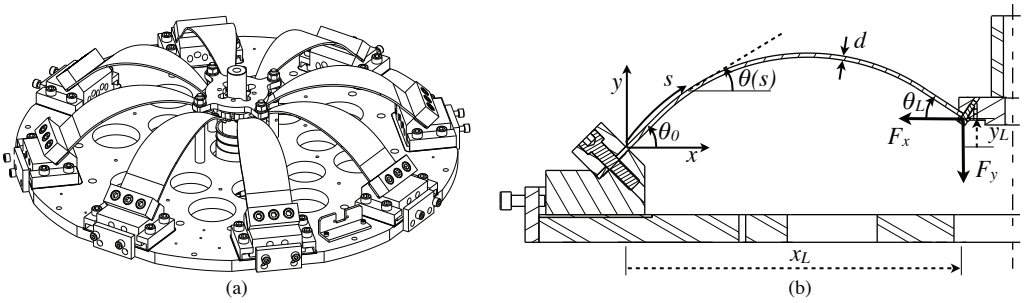

Fig. 2. a) A GAS filter. b) A schematic of a single GAS blade with relevant parameters.

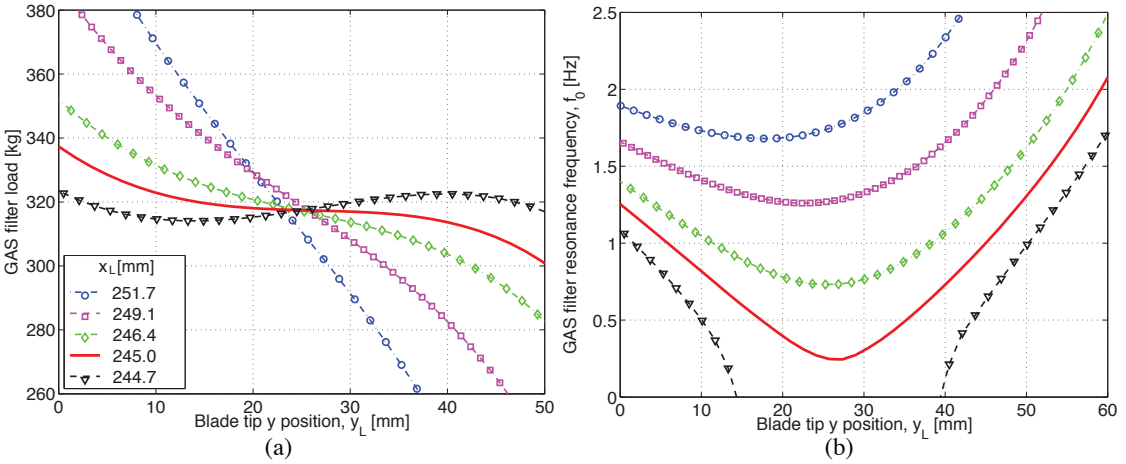

Fig. 3. a) Applied filter load versus the vertical position of the blade tip, for various compression distances x_L. A bistable state is evident for x_L = 244.7 mm. The red curve corresponds to a well-tuned GAS filter. b) Resonance frequency versus vertical position of the blade tip for various compression distances. Tuning the GAS spring involves finding a compression distance x_L that corresponds to the desired resonance frequency at the required load, whilst remaining stable.

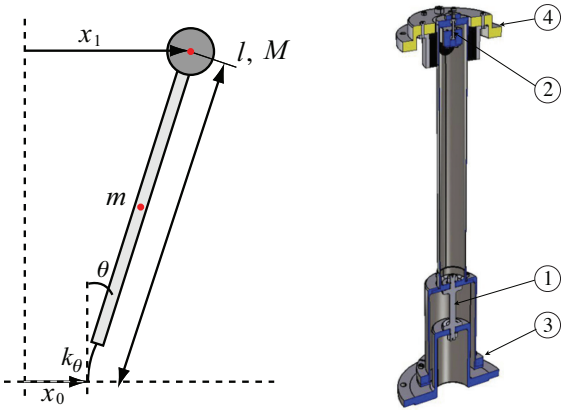

Fig. 4. Left: A schematic of a basic IP indicating the bending angle θ, mass M, of the payload supported by the IP, mass m of the IP leg. The IP is attached to the floor via a flexible joint with a spring constant, k_θ. The floor and payload displacement are given by x_0 and x_1 respectively. Typical values for EIB-SAS are l = 500 mm, m = 1.5 kg and M = 400 kg (per IP). Right: A cross-section of the IP installed in EIB-SAS. 1) Lower flexible joint. 2) Upper flexible joint. 3) Counter weights. 4) Spring box support.

This is achieved by an active control feedback system. The following section discusses the sensors used to observe the motion of the bench and the actuators used to apply a corrective force. Finally the control strategy and feedback system will be described.

3.1. Sensors and actuators

EIB-SAS is continuously monitored by two types of motion sensors: linear variable differential transformers (LVDTs) and velocity sensors called geophones. LVDTs measure displacements relative to a reference point, in this case the grounded plateau. Consequently, LVDTs can measure DC offset and low frequency displacement of the bench. For frequencies above the bench modes (> 1 Hz), the seismic motion of the grounded reference point will dominate the displacement signal. The LVDTs voltage output is linear to displacement within 1%, over a range of ±4 cm, providing an accuracy of a few nm.

Geophones are inertial sensors producing a voltage proportional to the velocity difference between its housing and an internally suspended reference mass. The voltage is induced in a pickup coil wound on the reference mass as it moves through a permanent magnet attached to the housing. The resonance frequency of the suspended mass system is usually in the order of a few Hz. Below the resonance frequency the geophone loses sensitivity due to the reference mass losing its inertial properties. The geophones signals are therefore valid from around 0.1 to 100 Hz.

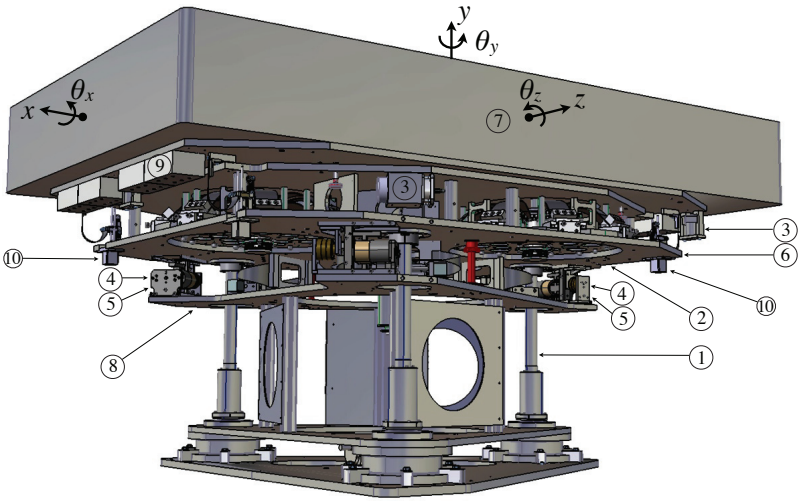

Fig. 5. An overview of EIB-SAS. 1) IP legs. 2) GAS springs. 3) Geophones (three vertical, three horizontal). 4) LVDT's (three vertical, three horizontal). 5) Actuators (three vertical, three horizontal). 6) Spring box. 7) Optical bench. 8) Grounded plateau 9) Balancing masses. 10) Stepping motors (four vertical, three horizontal).

Each of the LVDTs is co-located with co-axial voice coil actuators that allow control of the system as well as damping of modes. The geometry of the coil and magnetic yoke are designed to deliver constant force (within 1%) over a 10 mm movement range. The actuators are capable of positioning the optical table within the resolution of the LVDTs.

3.2. Control system

The EIB-SAS control system is governed by two main strategies; position and inertial control. LVDT signals are used to apply long-term position control to compensate for example, slow temperature and air pressure effects. A low-pass filter with a corner frequency around 0.1 Hz is used to prevent reference point displacements from spoiling performance at higher frequencies. Inertial control uses information from the geophones to feed back velocity signals, essentially applying a viscous damping to significantly reduce the quality factor of the resonance frequencies.

Because sensors and actuators are not in the same coordinate frame, transformations between frames need to be done, this is known as diagonalization [13–15]. Diagonalization combines the real sensor signals into virtual sensors that describe the motion in terms of relevant degrees of freedom (*xyz*-frame). This transformation is performed by the sensing matrix, **S**. The feedback signals are then computed in the usual way, only now for the virtual actuators corresponding to the virtual sensors. Again a transformation is required to obtain the real actuator signals, this is done with driving matrix, **D**. **S** and **D** are derived by measuring transfer functions between actuators and sensors. A schematic of the controls systems is given in Fig. 6.

The feedback compensator $C(s)$ varies for position and inertial control. It has been tuned for stability and performance. In the Laplace domain it can be described by,

$$C_{\text{position}}(s) = \frac{10s^2 + 1.5s + 0.3}{s + 0.01}\frac{C_0}{s^2 + 2s_0 s + s_0^2}, \qquad C_{\text{inertial}}(s) = C_0\frac{s^2}{(s+\omega_1)(s+\omega_2)}, \tag{4}$$

where C_0 is the feedback gain, s the Laplace variable $i\omega$ and s_0 the corner frequency of the second order low-pass filter. For the inertial controls the parameters ω_1 and ω_2 control the low and high frequency roll-off and should be chosen such that $\omega_1 \ll \omega_0 \ll \omega_2$. The simulation results of the closed and open-loop transfer functions of the above controls schemes are shown in Fig. 7a and 7b respectively.

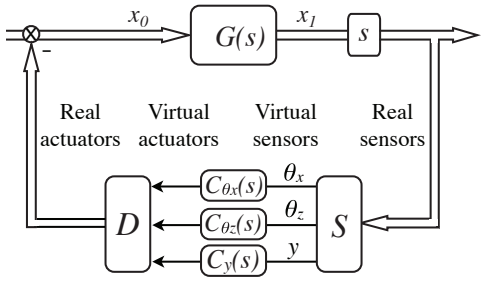

Fig. 6. Simplified schematic of the controls scheme, showing the sensing matrix **S** transforming the real sensor signals into virtual sensors. With the compensator of Eq. (4) the virtual feedback actuators signals are calculated before being transformed back to the real actuators signals via the driving matrix **D**.

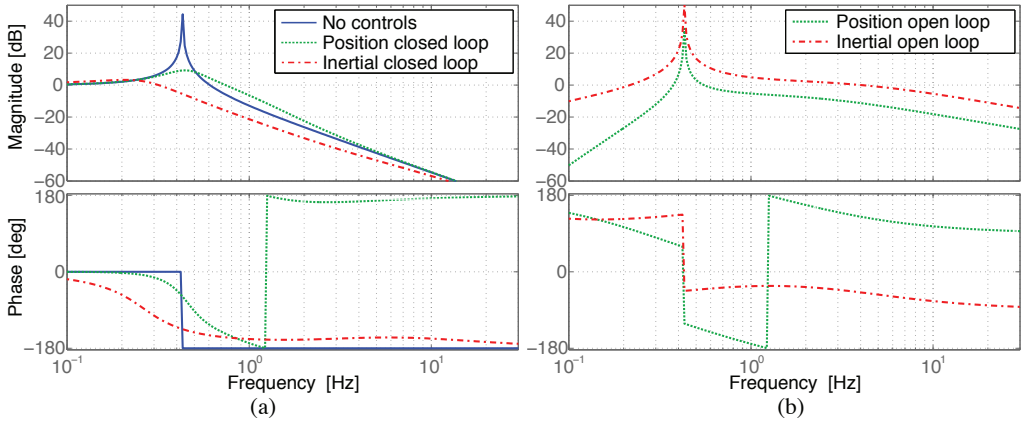

Fig. 7. a) Simulated open-loop transfer functions of EIB-SAS without controls, and with position (dotted green curve) and inertial (dashed red curve) damping. b) Respective closed loop transfer functions of the controls system.

4. Performance

This section will discuss the low frequency (< 10 Hz) performance of the bench starting by identifying the resonance modes and attenuation properties in an uncontrolled state. The modes are evident in the displacement spectra of LVDT signals plotted in Fig. 8a. The resonance peak of each degree of freedom is also indicated. Most spectra contain more than two resonance peaks, suggesting strong coupling between various modes. In Fig. 8b the transfer functions of the translational degrees of freedom are plotted. These were measured between two seismometers; one on the ground underneath, and the other on top of the optical bench. The rotational resonances are visible in the horizontal transfer function due to the seismometers sensitivity to rotational (tilt) motion. An attenuation of 40 dB is reached at 2 Hz for the horizontal directions and at 4 Hz vertically. Measuring in-air residual motion above 4 Hz is hampered by acoustic couplings and limited sensor sensitivity. Higher order modes of the system could affect performance in the detection band (> 10 Hz). Two such modes can be seen around 16 Hz that correspond to out of phase vibrations between the optical bench and spring box. The quality factors of higher order modes can be reduced significantly by extending the active controls bandwidth to include these frequencies or by using passive eddy current dampers. These issues will be addressed elsewhere [16].

Results of resonance damping using the inertial diagonalized control scheme are plotted in Fig. 9 for the vertical degrees of freedom. At least an order of magnitude damping is achieved in all cases without additional noise being injected at higher frequencies.

5. Conclusions

Seismic noise of optical benches induces noise in the output of the Virgo interferometric GW detector. This paper describes a passive seismic attenuation system that utilized the mechanical low-pass filter characteristics of harmonic oscillators to suppress the seismic motion of optical benches. EIB-SAS implements

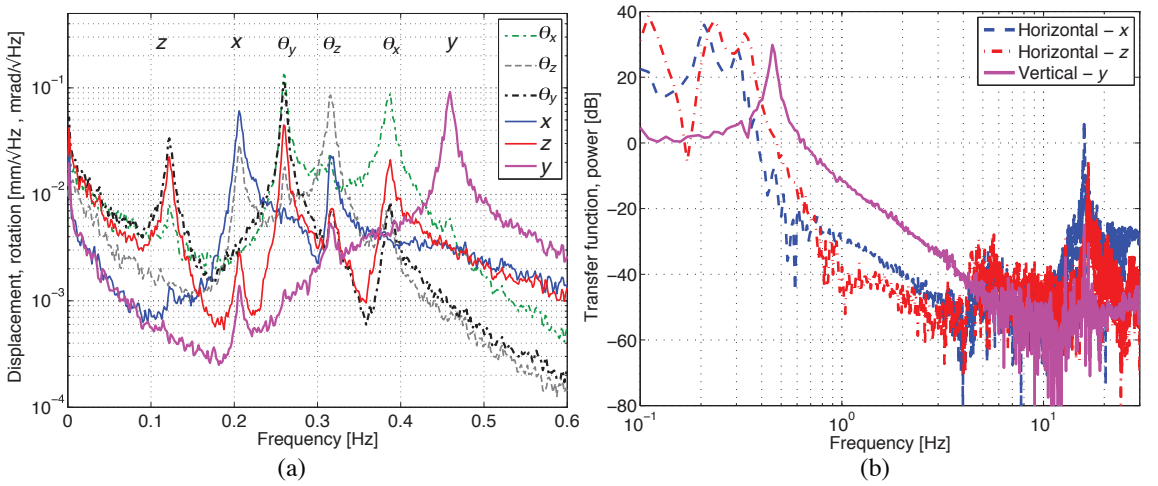

Fig. 8. a) Resonance frequencies of EIB-SAS. The 6 degrees-of-freedom can easily be distinguished. Strong coupling is evident by, for example, the large θ_y peak in the z degree of freedom (solid red curve). b) Transfer function of the translational degrees of freedom measured between seismometers underneath and on top of EIB-SAS. Tilt coupling into the seismometer signals is evident in the peaks at the angular resonances around 0.3 Hz. Above 4 Hz acoustic and instrumental noise start to dominate. Higher order mechanical modes of the system are visible around 16 Hz.

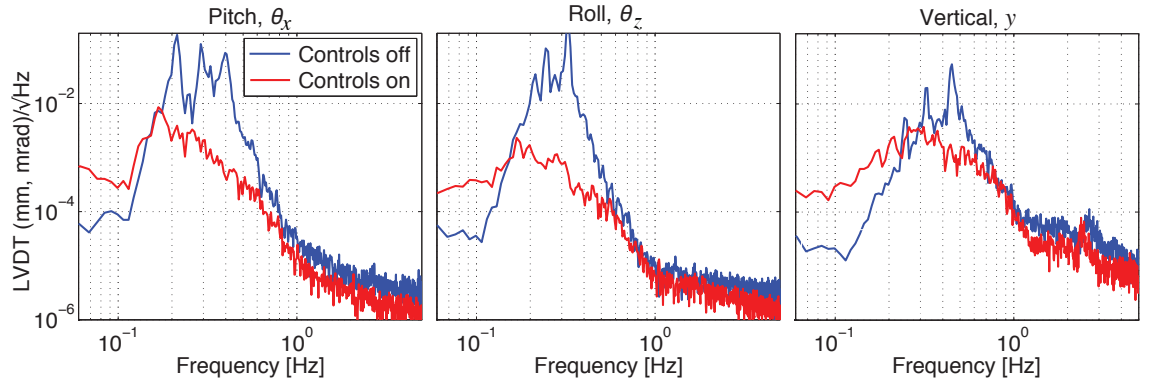

Fig. 9. Results of resonance damping using the inertial diagonalized control scheme for the vertical degrees of freedom. The control system is capable of suppressing the resonances by at least an order of magnitude.

anti-spring technology to allow for low resonance frequencies in combination with a compact design. In doing so, it has been shown that seismic attenuation of 40 dB is accessible above 4 Hz. Higher order modes and acoustic couplings need to be considered when accessing performance above 10 Hz. The resonance frequencies are damped with an active feedback system. Controls schemes using displacement and velocity sensors have been introduced. Results show that damping of these resonances by an order of magnitude can be achieved using inertial sensors. EIB-SAS was installed in Virgo at the end of 2011.

Acknowledgments

This work is part of the research program of the Foundation for Fundamental Research on Matter (FOM), which is financially supported by The Netherlands Organization for Scientific Research (NWO). We would like to thank Riccardo De Salvo and Alessandro Bertolini for their valuable input and discussions.

References

[1] F. Acernese, et al., Status of Virgo, Class. Quantum Grav. 25 (11) (2008) 114045.
[2] G. M. Harry, the LIGO Scientific Collaboration, Advanced LIGO: the next generation of gravitational wave detectors, Class. Quantum Grav. 27 (2010) 084006.
[3] H. Grote, the LIGO Scientific Collaboration, The GEO 600 status, Class. Quantum Grav. 27 (8) (2010) 084003.
[4] M. Beker, et al., Improving the sensitivity of future GW observatories in the 1-10 Hz band: Newtonian and seismic noise, General Relativity and Gravitation 43 (2011) 623–656.
[5] S. Braccini, et al., Measurement of the seismic attenuation performance of the Virgo superattenuator, Astroparticle Physics 23 (2005) 557–565.
[6] A. Seryi, O. Napoly, Influence of ground motion on the time evolution of beams in linear colliders, Phys. Rev. E 53 (1996) 5323–5337.
[7] A. Seryi, Investigations of slow motions of the Slac linac tunnel, in: 20th Inter. Linac Conf., 2000, arXiv:physics/0008195.
[8] F. Bondu, the VIRGO Collaboration, The Virgo injection system, Class. Quantum Grav. 19 (2002) 1829.
[9] T. Acadia, et al., Noise from scattered light in Virgo's second science run data, Class. Quantum Grav. 27 (2010) 194011.
[10] D. Macleod, et al., Reducing the effect of seismic noise in LIGO searches by targeted veto generation, arXiv:1108.0312v2 [gr-qc].
[11] I. Fiori, EIB seismic attenuation requirements for V+, Internal Virgo note, VIR-0601B-09 (2009).
[12] G. Cella, et al., Monolithic geometric anti-spring blades, arXiv:gr-cq 0406091v2 (2004) 502–519.
[13] G. Losurdo, Ultra-low frequency inverted pendulum for the Virgo test mass suspension, Ph.D. thesis, Pisa (1998).
[14] G. Losurdo, et al., Inertial control of the mirror suspensions of the Virgo interferometer for gravitational wave detection, Review of Scientific Instruments 72 (9) (2001) 3653–3661.
[15] R. Abbot, et al., Seismic isolation for Advanced LIGO, Class. Quantum Grav. 19 (2002) 1591–1597.
[16] M. Beker, A. Bertolini, M. Blom, J.F.J. van den Brand, H.J. Bulten, E. Hennes, EIB-SAS performance document, Internal Virgo note, VIR-0578B-11 (2011).